ACS NANO
Cite This: ACS Nano 2018, 12, 2634–2642
www.acsnano.org

ARTICLE

Thermal Transport in Quasi-1D van der Waals Crystal $Ta_2Pd_3Se_8$ Nanowires: Size and Length Dependence

Qian Zhang,[†,⊥] Chenhan Liu,[‡,⊥] Xue Liu,[§,⊥] Jinyu Liu,[§,⊥] Zhiguang Cui,[∥] Yin Zhang,[†,‡] Lin Yang,[†] Yang Zhao,[†] Terry T. Xu,[∥] Yunfei Chen,[‡] Jiang Wei,[§] Zhiqiang Mao,*[,§] and Deyu Li*[,†]

[†]Department of Mechanical Engineering, Vanderbilt University, Nashville, Tennessee 37235, United States
[‡]School of Mechanical Engineering and Jiangsu Key Laboratory for Design and Manufacture of Micro-Nano Biomedical Instruments, Southeast University, Nanjing 210096, PR China
[§]Department of Physics and Engineering Physics, Tulane University, New Orleans, Louisiana 70118, United States
[∥]Department of Mechanical Engineering and Engineering Science, The University of North Carolina at Charlotte, Charlotte, North Carolina 28223, United States

Supporting Information

ABSTRACT: Van der Waals (vdW) crystals with covalently bonded building blocks assembled together through vdW interactions have attracted tremendous attention recently because of their interesting properties and promising applications. Compared to the explosive research on two-dimensional (2D) vdW materials, quasi-one-dimensional (quasi-1D) vdW crystals have received considerably less attention, while they also present rich physics and engineering implications. Here we report on the thermal conductivity of exfoliated quasi-1D $Ta_2Pd_3Se_8$ vdW nanowires. Interestingly, even though the interatomic interactions along each molecular chain are much stronger than the interchain vdW interactions, the measured thermal conductivity still demonstrates a clear dependence on the cross-sectional size up to >110 nm. The results also reveal that partial ballistic phonon transport can persist over 13 μm at room temperature along the molecular chain direction, the longest experimentally observed ballistic transport distance with observable effects on thermal conductivity so far. First-principles calculations suggest that the ultralong ballistic phonon transport arises from the highly focused longitudinal phonons propagating along the molecular chains. These data help to understand phonon transport through quasi-1D vdW crystals, facilitating various applications of this class of materials.

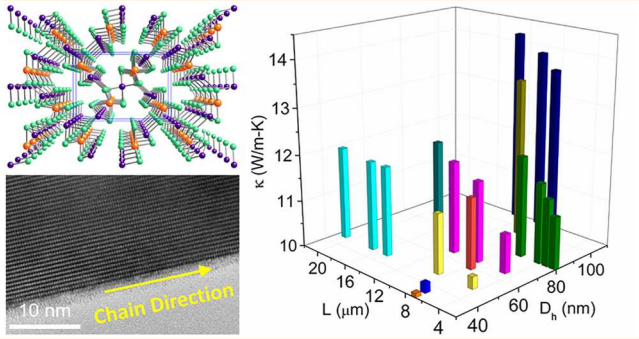

KEYWORDS: *van der Waals crystals, quasi-one-dimensional materials, thermal conductivity, phonon focusing, ballistic phonon transport*

The discovery of graphene[1] and other two-dimensional (2D) materials[2] has fueled enormous interests in exploration of van der Waals (vdW) nanomaterials and their properties. Similar to the case of graphite, whose successful exfoliation could lead to monolayer or few-layer graphene,[1] successful peeling of quasi-one-dimensional (quasi-1D) vdW crystals gives rise to quasi-1D vdW nanowires owing to their excellent scalability.[3−5] The quasi-1D structures could contribute to many interesting properties, such as topological insulator,[4] charge density waves,[5] and superconductor−insulator transitions.[6] They have also been demonstrated to have great potentials for practical applications, such as in thermoelectric devices[7] and transistors.[3,8] One particularly attractive application is as interconnects in nanoelectronics, taking advantage of their excellent scalability that does not suffer from the ever-escalating resistivity from miniaturizing the commonly used copper interconnects.[9,10]

Thermal properties of vdW crystals are of important considerations for many of their applications and have attracted significant attention.[11−16] Critical issues such as the effects of dimensionality and phonon focusing on thermal transport in these materials have been debated but a comprehensive understanding has not yet been achieved.[16,17] Moreover,

Received: December 9, 2017
Accepted: February 23, 2018
Published: February 23, 2018

DOI: 10.1021/acsnano.7b08718
ACS Nano 2018, 12, 2634–2642

while 2D vdW materials have been intensively studied,[16] thermal transport properties of quasi-1D vdW crystals have been rarely probed. Exploration of these materials systems could provide important insights into thermal transport in vdW crystals.[3,9,18]

The quasi-1D vdW crystals also make an excellent system for studying ballistic phonon transport. It has been predicted that for truly 1D materials, thermal conductivity could become divergent, manifested by the continuously increasing thermal conductivity with the sample length.[19,20] In reality, defects and Umklapp scattering can lead to finite thermal conductivity, and the thermal conductivity has been demonstrated to increase with sample length for up to 10 μm at room temperature for a single-walled carbon nanotube.[21] As such, it is interesting to examine the length dependence of the thermal conductivity of quasi-1D vdW materials to elucidate the effects of dimensionality and see how long ballistic phonon transport can persist in these materials. In view of the great potential of quasi-1D vdW crystals[9,10] and the importance of their thermal properties, here we report on the experimental study of the thermal conductivity of quasi-1D nanowires made of $Ta_2Pd_3Se_8$ (TPdS).

RESULTS AND DISCUSSION

Figure 1a depicts the highly anisotropic microstructure of TPdS, which consists of TPdS molecular chains (illustrated in Figure 1b and 1c) extending along the axial direction (*c*-axis) as the fundamental building blocks. The interchain interactions are mediated by vdW forces between the Pd and Se atoms of neighboring chains, which is calculated to be ~17 times weaker than the intrachain covalent bonds between Pd and Se from Liu *et al.*[3] It has been shown that individual molecular chains can extend along the *c*-axis up to centimeters, as determined from the synthesized centimeters long needle-like crystals.[3] Individual TPdS nanowires were prepared out of liquid exfoliations of single crystalline bulk specimen,[3,6,10] yielding single crystalline nanowires for experimental studies. As shown in Figure 1d, the chain structure can be clearly identified in high resolution transmission electron microscopy (HRTEM) examination of prepared nanowires.

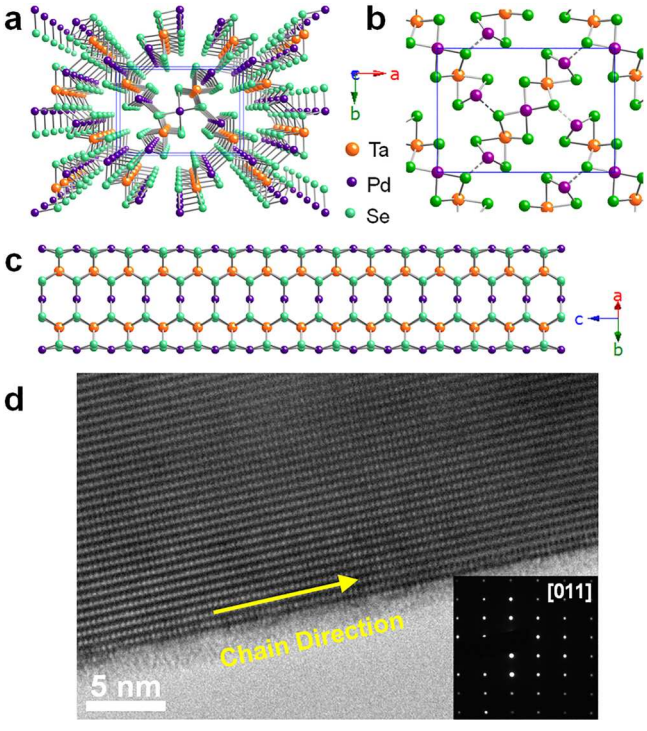

Figure 1. Crystal structure of TPdS nanowires. (a) Perspective view of bulk TPdS viewed along *c*-axis. (b) Planar schematic of cross-sectional view along *c*-axis. (c) Side-view of a molecule chain extending along *c*-axis. (d) HRTEM image showing perfectly aligned molecular chains. The inset is the diffraction pattern along the [011] crystalline direction, indicating the single crystalline nature.

Different from nanowires synthesized by chemical vapor deposition, the cross sections of these exfoliated quasi-1D vdW nanowires tend to be of rather irregular shapes. As such, we cut open the cross-section of the nanowires using focused ion beams (FIB) after first depositing a protection layer with electron beam induced deposition (EBID). High-resolution scanning electron microscopy (HRSEM) were then performed to reveal the cross-section of each tested nanowire (see details in Supporting Information Section III). The acquired SEM micrographs allow for extraction of the cross-sectional area and perimeter, enabling calculation of the surface-area-to-volume ratio (SVR), which has been shown to be a more proper parameter than the widely used Casimir length to characterize the classical size effects due to phonon-boundary scattering.[22,23] However, to present the size dependence in a more straightforward manner, we opt to use the hydraulic diameter (D_h) as the characteristic length of irregular cross-sectional nanowires, to gauge the cross-sectional size effects. The hydraulic diameter was calculated in the same manner as in fluid dynamics,[24] which equals to 4 times the reciprocal of SVR. For perfectly circular nanowires, the hydraulic diameter is the same as the Casimir length. However, for nanowires of noncircular cross sections, Casimir length was calculated by assuming a circular cross section of equivalent area, which does not accurately account for the boundary effects in nanowires of irregular cross sections.[24,25] In fact, based on the Casimir length, the size effects should be the same for nanowires of identical cross-sectional areas, which has been proven to be inaccurate by one recent study on silicon nanoribbons of different aspect ratios.[22] Different cross-sectional shapes, even of the same cross-sectional area, can lead to different ribbon thermal conductivity. The SVR, on the other hand, has been shown to better reflect the surface effects; and therefore, adopting the hydraulic diameter, which is inversely proportional to SVR, could provide a more accurate means to quantify size effects in our case.

Contact Thermal Resistance and Electronic Thermal Conductivity. The inset in Figure 2a shows a single TPdS nanowire situated between two suspended membranes with integrated platinum (Pt) coils serving as resistance heaters and thermometers, facilitating simultaneous measurement of thermal and electrical conductivity.[26] Contact resistance in thermal/electrical property measurement needs to be carefully taken care of in order to produce reliable experimental results.[27,28] This is especially true for examining the length-dependence of thermal conductivity, as non-negligible contact thermal resistance could lead to artifacts and erroneous conclusions.[29] In our case, EBID of Pt has been done to minimize the electrical and thermal contact resistance as shown in the inset of Figure 2a. Importantly, the contact thermal resistance has been confirmed to be negligible by comparing the measured thermal conductance after the first and second

DOI: 10.1021/acsnano.7b08718
ACS Nano 2018, 12, 2634−2642

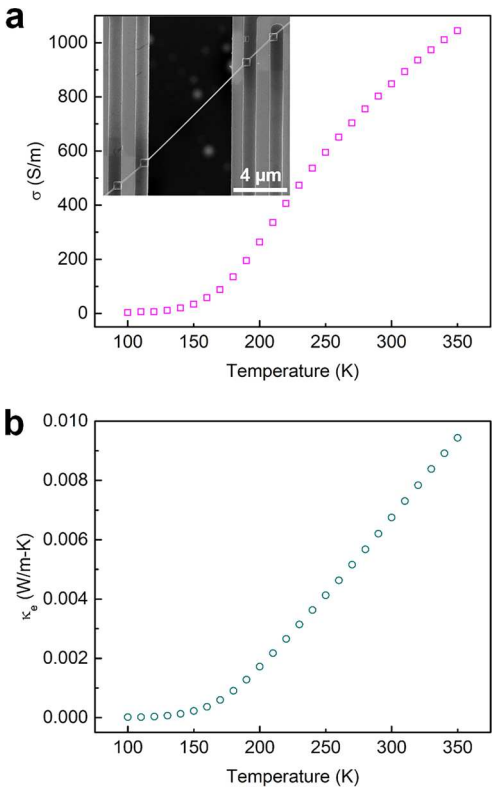

Figure 2. Evaluation of the electronic thermal conductivity of a TPdS nanowire. (a) Measured electrical conductivity of a TPdS nanowire of 96 nm hydraulic diameter and (b) the corresponding estimated electronic thermal conductivity k_e. The inset in (a) displays an SEM micrograph of the TPdS nanowire showing that the wire is bonded to four electrodes on the measurement device with EBID of Pt, allowing for four-probe measurement of its electrical resistance.

rounds of EBID, which yielded essentially the same measurement results (see Supporting Information Section II). It has been shown that if the contact thermal resistance is not negligible, the measured thermal conductance will change with additional Pt deposition.[30] To explore the length dependence of the thermal conductivity, the same nanowire can be cut mechanically using a sharp probe and resuspended for several times with the length of the suspended section ranging from 2 to 21 μm.[17,27,31] We note that the confirmation of negligible contact thermal resistance post EBID contact treatment is done with a relatively short suspended wire length (3.2 μm long); and for longer suspended lengths, the effects of contact thermal resistance become even smaller as the intrinsic resistance of the wire gets larger.

Both electrons and phonons can contribute to thermal transport in TPdS. To evaluate the contribution of electrons to thermal transport, we measured the electrical conductivity of one TPdS nanowire as shown in Figure 2 (the inset in Figure 2a shows the SEM image of the wire). The extracted electrical conductivity increases with temperature, indicating the semiconducting nature of the material. The electron contribution to the thermal conductivity, k_e, can then be estimated following the Wiedemann–Franz Law as $k_e = L\sigma T$, in which σ is electrical conductivity, T is temperature, and $L = 2.44 \times 10^{-8}$ WΩ/K^2 is the Lorenz number. The calculated k_e is plotted in Figure 2b, displaying an escalating trend as temperature increases. The data indicate that even at 350 K, where the electrical conductivity is the highest, k_e is still very small (~0.01 W/m K), about 3 orders of magnitude less than the measured k at 350 K (~12.6 W/m K). In fact, the electrons contribute to no more than 0.2% of the total thermal conductivity over the whole measurement temperature range, indicating the negligible role of electrons in carrying heat in TPdS. Therefore, in following analysis we attribute the measured thermal conductivity to phonons, and neglect the contributions from electrons.

Cross-Sectional Size Dependence. Since the intrachain covalent bonding between Pd and Se is much stronger than the interchain vdW interactions between the Pd and Se residing on neighboring chains, it is interesting to see whether the thermal conductivity of TPdS nanowires still displays a dependence on the cross-sectional size. Figure 3a plots the measured thermal conductivity *versus* temperature for four samples of different D_h, which indicates that even for such highly anisotropic quasi-1D vdW nanowires, the thermal conductivity still exhibits a clear size dependence. Note that since the length of the nanowires could also have an effect, we select samples of similar lengths for this comparison and make sure that nanowires of larger D_h are of shorter suspension lengths. This way, any effect from the

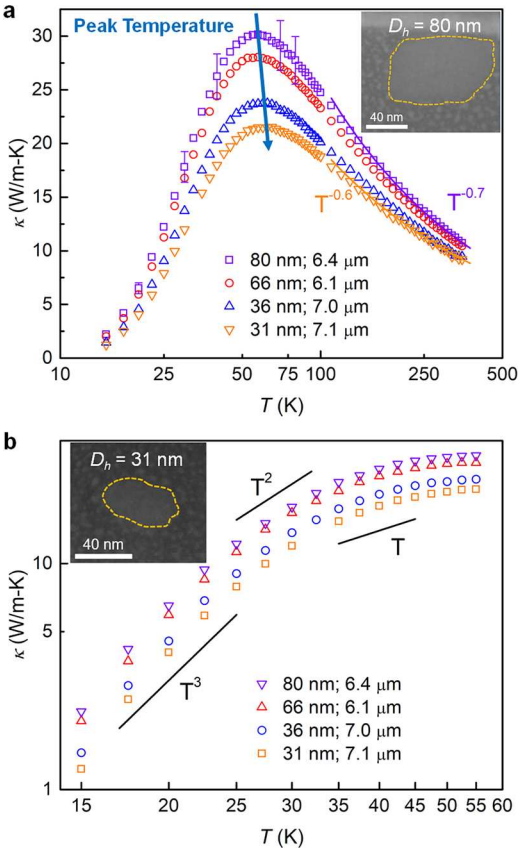

Figure 3. Size-dependent thermal conductivity of TPdS nanowires. (a) Thermal conductivity of TPdS nanowires in full temperature range from 15 to 350 K, showing strong size dependence. For the sake of clarity, only five error bars are shown for the 80 nm sample in purple. (b) Low temperature thermal conductivity of nanowires of varying hydraulic diameters. The curves of T,[3] T^2, and T^1 are also shown for comparison. The insets are the HRSEM images showing the irregular cross sections of two selected nanowires of different hydraulic diameters, whose contours were outlined by the dashed yellow lines.

DOI: 10.1021/acsnano.7b08718
ACS Nano 2018, 12, 2634–2642

length difference will only counter the trend of size dependence, so the actual thermal conductivity enhancement for larger cross-sectional size will be more significant.

The nanowires with larger D_h, which correspond to larger cross-sectional areas and smaller SVRs, possess higher thermal conductivity. In fact, this cross-sectional size dependence can persist up to a D_h of 110 nm, as shown later, which is not as expected based on the behavior of 2D vdW materials. For most well-studied 2D vdW materials, including graphene,[15] h-BN,[32] and MoS_2,[33] their in-plane thermal conductivity decreases as the thickness increases from monolayer to few layers. Particularly, for multilayer graphene, the thermal conductivity quickly reaches bulk values when the number of layers increases to merely ∼5, at which point the disturbance from the weak interlayer vdW interactions to phonons propagating within each layer saturates.[15] Similar physics have been argued for ideally oriented 1D polyethylene as well based on molecular dynamics results.[34] We note that for some other 2D vdW materials, such as black phosphorus, their thermal conductivity have been shown to increase with the number of layers but quickly saturate to bulk values when the layer thickness reaches ∼10 nm.[35] In general, for 2D vdW materials, the size dependence becomes marginal for samples when their thickness is beyond ∼10 nm; and therefore, the observed size dependence for the TPdS nanowires with hydraulic diameter up to >110 nm is counterintuitive.

To understand the above cross-sectional size dependence of the thermal conductivity, we first examine the temperature dependence of the thermal conductivity at low temperature, which follows the Debye T^3 law between 15 to 25 K (Figure 3b), different from the expected linear relationship for 1D material systems such as single wall carbon nanotubes.[36] We note that for graphite, the most popular 2D vdW material, its heat capacity also obeys the T^3 law below 10 K, as a result of the contribution of both intra- and interlayer phonon modes. The trend then transitions to T^2 from 10 to 100 K, when the in-plane phonon modes start to dominate over the low energy cross-plane modes sustained by weak vdW interactions.[37,38] Compared to graphite, which has an interlayer bonding energy of ∼0.05 eV,[38] the interchain bonding energy formed between neighboring Pd and Se on different molecular chains for TPdS is significantly higher, ∼0.34 eV,[3] which can sustain the propagation of interchain phonon modes of higher energy. The extended temperature range in which the T^3 law holds for TPdS nanowires is therefore a direct result of this enhanced interchain interaction strength that allows for higher frequency interchain phonons. As such, the interchain phonon modes should be able to make more contributions to thermal transport in TPdS than the interlayer phonon modes in graphite. On the other hand, the much more atoms (26) in each unit cell of TPdS generate more optical phonon modes, facilitating the occurrence of Umklapp scattering. In addition, the much heavier atoms and larger unit cells give rise to significantly lower speed of sound along the chain (denoted as the *c*-axis). As a result, the along-chain thermal conductivity for TPdS nanowires is 2 orders of magnitude lower than the in-plane thermal conductivity of graphite. Together, the much-enhanced interchain interaction and the significantly reduced contribution of intrachain phonon modes to thermal transport result in a significant weight in the *c*-axis thermal conductivity from phonons not propagating along the molecular chains, which is responsible for the observed cross-sectional size dependence.

Another challenge here is that for above argument to be true, the phonons propagating not along the *c*-axis need to possess large enough mean free paths (MFPs), comparable to the D_h of >110 nm. Even though traditionally it has been believed that vdW interactions correspond to small phonon MFPs, we believe that this is not necessarily the case given the recent demonstration of the very long phonon MFP along the *c*-axis (cross plane direction) of graphite, which is ∼200 nm at room temperature, 2 orders of magnitude larger than the often cited value of merely a few nanometers.[17,39−41] Therefore, it is reasonable to conclude that the MFP of phonons in TPdS nanowires is longer than 110 nm.

All four measured nanowires in Figure 3a demonstrate a similar temperature dependence. Their thermal conductivity ramps up quickly with increasing temperature from 15 K, reaching a peak value around 55 K, and then decreases as the temperature further rises, which is a signature of Umklapp scattering. As the temperature rises beyond 100 K, the thermal conductivity displays a trend of $T^{-0.6-0.7}$, with the exponent dropping from −0.6 to −0.7 as the wire cross-sectional size increases, approaching the T^{-1} behavior for bulk single crystalline materials. The slower drop rate can be attributed to phonon boundary scattering in nanowires; which also leads to a shift of the peak thermal conductivity toward higher temperature for nanowires of smaller D_h, similar to that for silicon nanowires/ribbons.[22,42] As discussed later, ballistic phonon transport along the wire axial direction still makes significant contribution in these 6−7 μm long wires so boundary scattering at the two ends of the nanowires also contributes to the deviation from the T^{-1} behavior.

Length Dependence. Beyond the cross-sectional size dependence, exploration of the *c*-axis thermal conductivity as a function of the sample length to probe ballistic phonon transport along the chain in this quasi-1D material system also holds great interests.[20] To accomplish this study, we have measured the same nanowire (D_h = 66 nm) with different lengths suspended between the heat source and sink, as shown in Figure 4a−c. As shown in Figure 4d, the measured thermal conductivity displays a clear dependence on the sample length as it varies from 4.9 to 11.2 μm, with higher thermal conductivity for longer suspension length. This trend holds even at the rather high temperature of 350 K, as demonstrated in Figure 4e. This length dependence indicates rather persistent ballistic phonon transport along the chain direction and invokes an interesting question: what is the limit of the ballistic transport length for thermal phonons in these quasi-1D nanowires? Furthermore, considering the cross-sectional size dependent thermal conductivity shown in Figure 3, will the length dependence persist even longer for nanowires of even larger cross sections?

To explore this limit, we measured the thermal conductivity of several nanowires of different suspended lengths and different hydraulic diameters. Since the thermal conductivity varies with the wire cross-section, to ensure a meaningful comparison, either a very long nanowire was cut into several segments for different suspended lengths or a relatively long nanowire underwent cutting and resuspension several times (Figure 4). Figure 5 plots the room temperature (300 K) thermal conductivity *versus* the nanowire length and hydraulic diameter. From Figure 5, it can be clearly discerned that, for nanowires of similar length, the dependence on the hydraulic diameter persists for nanowire up to 110 nm. Furthermore, both Figure 5 and Figure S3b show that the length dependence

DOI: 10.1021/acsnano.7b08718
ACS Nano 2018, 12, 2634−2642

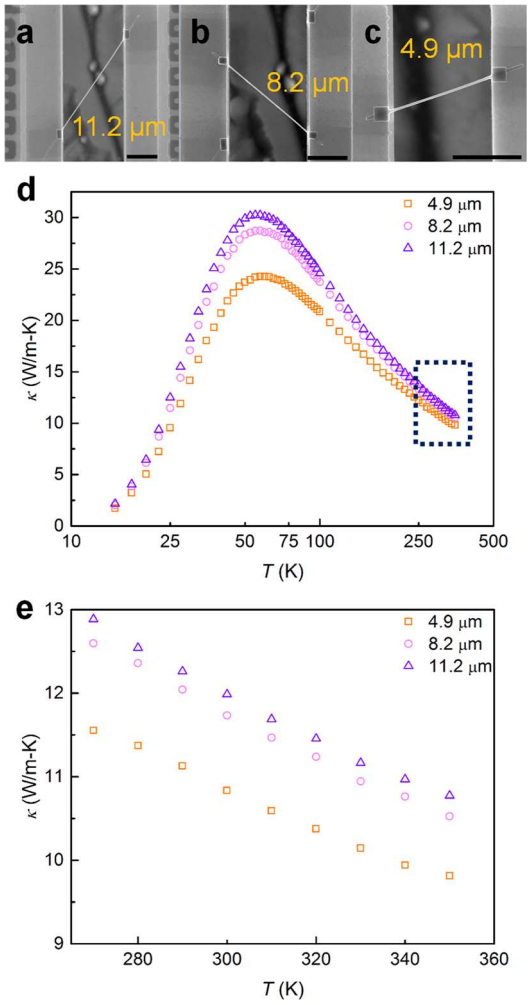

Figure 4. Length dependence of the thermal conductivity of one TPdS nanowire. (a–c) The same nanowire (D_h = 66 nm) was cut and suspended for different lengths of 11.2 μm, 8.2 μm, and 4.9 μm, respectively. The scale bars all denote 3 μm. (d) Measured thermal conductivity of one nanowire for three different suspended lengths plotted against temperature ranging from 15 to 350 K. (e) Zoom-in view of the high temperature thermal conductivity from 270 to 350 K.

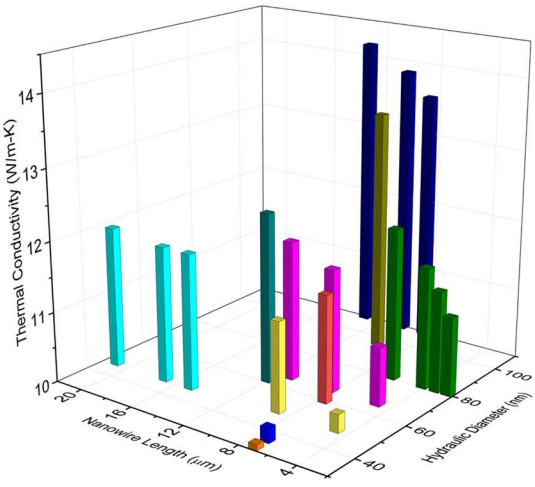

Figure 5. Room temperature (300 K) thermal conductivity of several TPdS nanowires plotted against nanowire suspension length and hydraulic diameter. The data from each nanowire are separately identified by different color and the data points from the same nanowire are in the same color. The general ascending thermal conductivity with increasing suspended length and larger diameter suggests existence of ballistic phonon transport up to 13 μm at 300 K and size dependence up to a hydraulic diameter >110 nm.

preserves up to 13 μm at 300 K, which is rather surprising, considering the low onset temperature of Umklapp scattering of ~55 K. Notably, this value is significantly larger than the demonstrated 8.3 μm length dependence in SiGe nanowires,[43] and ~10 μm for single wall carbon nanotubes.[21] This observation is also quite unexpected given the clear thermal conductivity dependence on the cross-sectional size, indicating the significant role of phonon scattering at nanowire surface. At 55 K (peak temperature), as shown in Figure S3a the length dependence could extend up to a length of 17 μm when phonon–phonon Umklapp scattering becomes weaker (see Supporting Information Section IV). This dependence indicates that the along-chain vibrations must also contribute a significant portion to the nanowire thermal conductivity and these vibration modes can propagate persistently over a long distance before Umklapp scattering or boundary scattering at the nanowire ends occurs. Importantly, the systematic dependence showcased in Figure 5 strongly suggests that the length dependence is not due to non-negligible contact thermal resistance. Contact thermal resistance can vary from sample to sample, which is especially true for wires of irregular cross sections, and if it plays a big role in the length dependence, then it is highly unlikely that the measured data will display the systematic trend as shown in Figure 5.

First-Principles Calculation of Thermal Transport in TPdS. To gain a better understanding of the interesting dependence on both the cross-sectional size and the nanowire length, an in-depth knowledge of the phonon transport characteristics of TPdS is required. Unfortunately, such information is not readily available in literature. Therefore, we conducted first-principles calculation to extract its elastic constants and thermal conductivity to probe phonon transport in this highly anisotropic material (see Supporting Information Section V for more details of modeling). Figure 6a shows the cross-sectional view of TPdS in the simulation domain, and the symbols *a* and *b* denote two interchain directions, with *c* representing the along-chain direction. Figure 6b plots the thermal conductivity of a 40 nm diameter nanowire of circular cross-section together with the bulk thermal conductivity from the modeling, in comparison with the experimental data for a nanowire of a similar hydraulic diameter of 36 nm and of 7 μm in length. Several observations can be obtained from this figure. First, the predicted thermal conductivity for the 40 nm diameter nanowire is signficantly lower than the bulk value, which is consistent with the experimentally observed size dependence on the cross-section. In addition, the temperature dependence of the predicted thermal conductivity demonstrates a trend that is very similar to that of the experimental data in the temperature range beyond 50 K, suggesting that our modeling reasonably capture the key features of phonon transport in TPdS. However, the predicted thermal conductivity is about 40% higher than the experimental data, which likely comes from factors such as the slightly larger diameter of the modeled wire, shorter length of the experimentally tested nanowire, and the difficulty of accurately taking into account all phonon properties in such complex materials. We note that with the large number of atoms in the unit cell (26), the first-

DOI: 10.1021/acsnano.7b08718
ACS Nano 2018, 12, 2634–2642

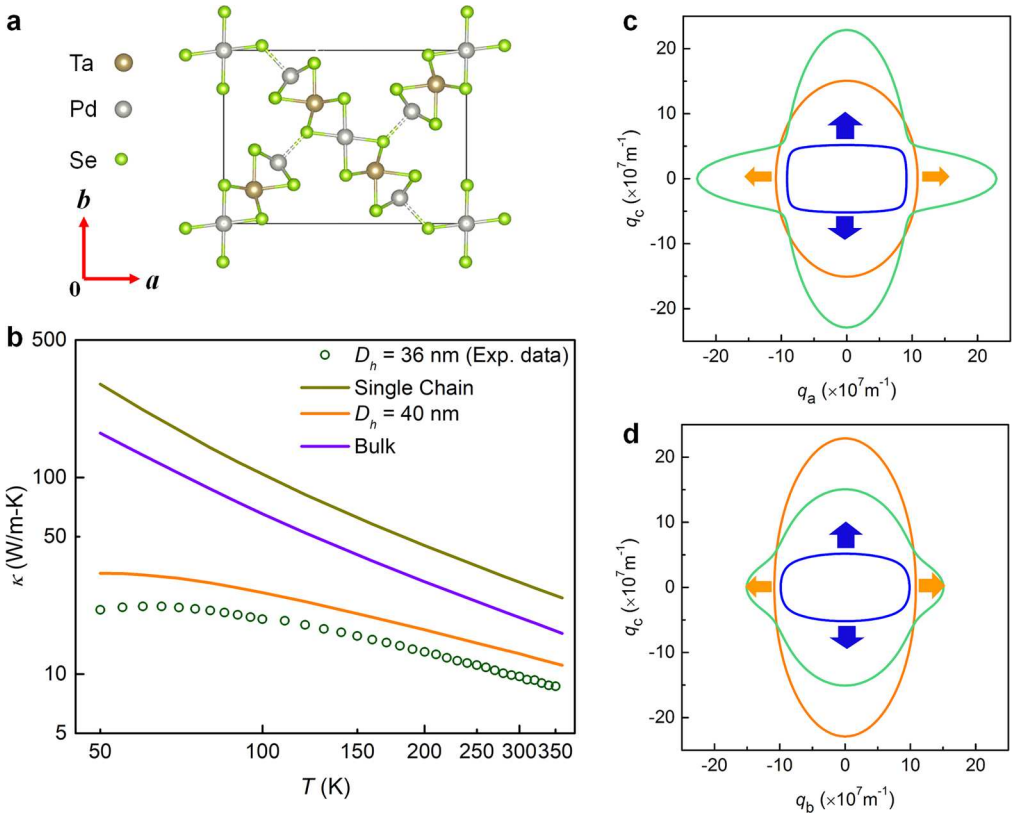

Figure 6. Calculated thermal conductivity and projected iso-energy surfaces of TPdS. (a) Unit cell for first-principles calculation. (b) Calculated thermal conductivity of bulk, a 40 nm nanowire, and a single chain in comparison to experimental data of one 36 nm nanowire. Iso-energy surfaces for longitudinal acoustic phonons (blue, innermost) and two types of transverse phonons (orange and green, outer two) of frequency 0.2 THz in (c) *ac*-plane and (d) *bc*-plane. The arrows indicate the directions along which phonons are focused to propagate.

principles calcualtion is quite demanding on the computational power and only a limited number of unit cells can be considered.

To consider the effects of interchain interactions, we also calculated the thermal conductivity of a single molecular chain using the obtained phonon dispersion curves along the *c*-axis direction. Figure 6b indicates that the thermal condcutivity of a single molecular chain should still be higher than the calculated bulk value. This behavior, similar to the cases of polyethylene molecular chains[34] and graphene,[15] derives from the fact that interchain interactions could incur significant scatterings to the intrachain phonon modes. The simulation results, together with the experimental data, suggest an interesting trend that the thermal conductivity of these TPdS nanowires would decrease sharply as the molecular chains stack together from a single chain to multiple chains due to disturbance to the propagation of intrachain phonon modes from interchain interactions, similar to that for few-layer graphene or polyethylene molecular chains.[34] The enhanced anharmonic scattering, however, quickly saturates as several chains assemble together, while interchain phonon modes start to be excited and make contributions to the thermal conductivity. As more molecular chains assembled together and the wire diameter increases, more interchain phonon modes are allowed and the MFP of these phonons increases with the cross-sectional size, which eventually gives rise to the observed size dependence of thermal conductivity on the cross-section in our experiment as a result of the classical size effect for nanowires.[22,42]

In order to further visualize the anisotropy of phonon transport, the iso-energy surfaces[44] of longitudinal and transverse phonons of 0.2 THz frequency are calculcated for *ac*- and *bc*- planes, respectively. As shown in Figure 6c,d, the longitudinal acoustic phonons are highly focused with one propogation direction nearly perfectly aligned with the *c*-axis direction, which originates from the strong convalent bonds in this direction. The two transverse acoustic phonon modes, however, demonstrate less anisotropy, and the effects of phonon focusing are significantly weaker than the longitudinal phonons. Note that even in the plane perpendicular to the *c*-axis, because of the different interatomic strengths along the *a*- and *b*-directions, there still exists some anisotropy, especially with respect to the two transverse phonon modes.

The strong dependence of the *c*-axis thermal conductivity on the cross-sectional size indicates that phonon boundary scattering is still highly effective in reducing the MFP of phonons in these quasi-1D vdW TPdS nanowires. As such, the observed persistent ballistic transport of thermal phonons in the wire axial direction has to come from phonons that transport along the wire axial direction. The iso-energy surfaces disclosed in Figure 6c,d suggest that due to the strong elastic anisotropy, longitudinal phonons are highly focused along the molecular chain axis. These phonons therefore suffer miminal boundary scattering, leading to preservation of the bulk longitudinal phonon MFPs along the *c*-axis direction, and showcasing the ascending thermal conductivity with longer nanowire length up to 13 μm. This is very different from elastically more isotropic materials, such as silicon. It has been shown that for bulk silicon more than half of heat conduction comes from phonons of MFPs longer than 1 μm and approximately 20% of the heat is conveyed by phonons with

DOI: 10.1021/acsnano.7b08718
ACS Nano 2018, 12, 2634−2642

MFPs beyond 10 μm at room temperature.[45] However, ballistic phonon transport in silicon nanostructures has been shown to be limited to sub-μm at room temperature[46] and only reached ~3 μm at 4 K,[47] due to strong boundary scattering of isotropically propagating phonons. One more factor that might contribute to the long ballsitic transport distance of thermal phonons along the TPdS nanowires is that the heavy atoms and the complex unit cell renders the acoustic phonons contributing to thermal transport in the TPdS more heavily weighted in the low- to medium-frequency range, which also likely to travel longer distance without being scattered.[48] All these factors working in concert to contribute to the observed ultralong ballistic phonon transport distance along the molecular chain direction.

CONCLUSIONS

In summary, we present a systematic experimental study of the thermal conductivity of quasi-1D single-crystalline vdW TPdS nanowires. The experimental data reveal significant dependence of the thermal conductivity on the cross-sectional size up to >110 nm, which arises from the important contribution of interchain phonon modes that are subjected to phonon boundary scattering. The results also indicate that partial ballistic transport of thermal phonons can persist for a long distance of up to 13 μm at room temperature and up to 17 μm at 55 K along the axial direction of nanowires. Analysis based on first-principles calculations suggests that this superlong ballistic transport was facilitated by nearly perfect alignment of longitudinal phonons with the molecular chain direction. These findings help to disclose thermal transport mechanisms in quasi-1D vdW nanomaterials and provide essential thermal property data for further exploitation of this class of materials for practical applications such as in thermoelectric energy conversion and interconnects in nanoelectronic devices.

METHODS

Preparation of Individual TPdS Nanowires for Thermal Measurements. Single crystal bulk sample of TPdS were grown using chemical vapor transport (CVT). TPdS nanowires were prepared by liquid exfoliation of the as-acquired bulk sample, using isopropyl alcohol (IPA) as solvent through sonication (see more in Supporting Information Section I). Nanowires acquired through direct exfoliation of high quality bulk materials are single crystals, making excellent specimens for transport property characterization. The obtained nanowire suspension was then diluted and drop-casted onto a polydimethylsiloxane (PDMS) substrate. After the solvent evaporated, individual nanowires were selected, picked up using a sharp probe mounted on a micromanipulator, and transferred to a microdevice for subsequent thermal property measurement. EBID of Pt was done using a dual beam system (FIB/SEM, FEI Helios NanoLab G3) to minimize the contact thermal resistance and establish good electrical contacts (inset of Figure 2a).

Thermal Conductivity Measurements. Thermal conductivity measurements were conducted in a cryostat (Janis CCS-400/204) operated under high vacuum ($<1 \times 10^{-6}$ mbar) with a dual radiation shield configuration, following the general procedure that has been successfully employed to study various nanowires and nanotubes.[22,26,30,49−51] The contact thermal resistance has been confirmed to be negligible by comparing the measured thermal conductance after the first and second rounds of EBID, which yielded essentially the same measurement results (see Supporting Information Section II).[30]

To visualize the cross-section of the exfoliated nanowires, we first used EBID to deposit a layer of Pt on the nanowire and then applied a high ion current to cut open the cross-section. The deposited Pt served as an anchor and a protective layer to prevent damage of the nanowire surface during the cutting process. The exposed cross-section was then subjected to HRSEM imaging (see the insets in Figure 3 and Supporting Information Section III), from which the cross-sectional area is extracted from the ImageJ software.

Uncertainty Analysis. The uncertainty of cross-sectional area is conservatively estimated to be less than 10%. The uncertainty from electrical measurement has been evaluated to be less than 2% following a Monte Carlo method,[52] and the uncertainty from the length measurement is conservatively estimated as 200 nm. The overall uncertainty of thermal conductivity was calculated following the equation of uncertainty propagation.[52]

ASSOCIATED CONTENT

Supporting Information

The Supporting Information is available free of charge on the ACS Publications website at DOI: 10.1021/acsnano.7b08718.

Additional synthesis, contact thermal resistance characterization, cross-sectional characterization, and first-principles modeling details (PDF)

AUTHOR INFORMATION

Corresponding Authors

*E-mail: zmao@tulane.edu.
*E-mail: deyu.li@vanderbilt.edu.

ORCID

Qian Zhang: 0000-0002-2692-9729
Lin Yang: 0000-0003-4838-5213
Yunfei Chen: 0000-0002-8682-868X
Deyu Li: 0000-0001-8364-0924

Author Contributions

⊥Q.Z., C.L., X.L., and J.L. contributed equally to this work. Q.Z., X.L., and J.L. initiated the project. J.L. synthesized the bulk TPdS. X.L. prepared the nanowires. Q.Z. conducted thermal conductivity measurements. C.L. carried out the first-principle and iso-energy surface calculation. Z.C. performed the TEM characterization. Q.Z. and D.L. wrote the manuscript. Q.Z., C.L., X.L., J.L., L.Y., T.X., J.W., Z.M. and D.L. edited the manuscript. D.L. supervised the project. All authors discussed the results and commented on the manuscript.

Notes

The authors declare no competing financial interest.

ACKNOWLEDGMENTS

The authors thank the financial support from the U.S. National Science foundation (DMR-1308550, DMR-1308509, CBET-1403456, DMR-1532107), as well as the Naval Engineering Education Consortium (NEEC) program (contract#: N00174-16-C-0008). Work at Tulane University was supported by the U.S. Department of Energy under Grant DE-SC0014208 (support for crystal growth and characterization) and Louisiana Board of Regents under Grant LEQSF (2015-18)-RD-A-23. C.L. acknowledges financial support from the Fundamental Research Funds for the Central Universities and the Innovative Project for Graduate Students of Jiangsu Province (Grant No. KYLX15_0058) and National Natural Science Foundation of China (51435003).

REFERENCES

(1) Novoselov, K. S.; Geim, A. K.; Morozov, S. V.; Jiang, D.; Zhang, Y.; Dubonos, S. V.; Grigorieva, I. V.; Firsov, A. A. Electric Field Effect in Atomically Thin Carbon Films. *Science* **2004**, *306*, 666−669.
(2) Butler, S. Z.; Hollen, S. M.; Cao, L.; Cui, Y.; Gupta, J. A.; Gutiérrez, H. R.; Heinz, T. F.; Hong, S. S.; Huang, J.; Ismach, A. F.;

DOI: 10.1021/acsnano.7b08718
ACS Nano 2018, 12, 2634−2642

Johnston-Halperin, E.; Kuno, M.; Plashnitsa, V. V.; Robinson, R. D.; Ruoff, R. S.; Salahuddin, S.; Shan, J.; Shi, L.; Spencer, M. G.; et al. Progress, Challenges, and Opportunities in Two-Dimensional Materials Beyond Graphene. *ACS Nano* **2013**, *7*, 2898−2926.
(3) Liu, X.; Liu, J.; Antipina, L. Y.; Hu, J.; Yue, C.; Sanchez, A. M.; Sorokin, P. B.; Mao, Z.; Wei, J. Direct Fabrication of Functional Ultrathin Single-Crystal Nanowires from Quasi-One-Dimensional van Der Waals Crystals. *Nano Lett.* **2016**, *16*, 6188−6195.
(4) Autès, G.; Isaeva, A.; Moreschini, L.; Johannsen, J. C.; Pisoni, A.; Mori, R.; Zhang, W.; Filatova, T. G.; Kuznetsov, A. N.; Forró, L.; Van den Broek, W.; Kim, Y.; Kim, K. S.; Lanzara, A.; Denlinger, J. D.; Rotenberg, E.; Bostwick, A.; Grioni, M.; Yazyev, O. V. A Novel Quasi-One-Dimensional Topological Insulator in Bismuth Iodide β-Bi_4I_4. *Nat. Mater.* **2016**, *15*, 154−158.
(5) Hor, Y. S.; Xiao, Z. L.; Welp, U.; Ito, Y.; Mitchell, J. F.; Cook, R. E.; Kwok, W. K.; Crabtree, G. W. Nanowires and Nanoribbons of Charge-Density-Wave Conductor $NbSe_3$. *Nano Lett.* **2005**, *5*, 397−401.
(6) Ning, W.; Yu, H.; Liu, Y.; Han, Y.; Wang, N.; Yang, J.; Du, H.; Zhang, C.; Mao, Z.; Liu, Y.; Tian, M.; Zhang, Y. Superconductor−Insulator Transition in Quasi-One-Dimensional Single-Crystal Nb_2PdS_5 Nanowires. *Nano Lett.* **2015**, *15*, 869−875.
(7) Chung, D.-Y.; Hogan, T.; Brazis, P.; Rocci-Lane, M.; Kannewurf, K.; Bastea, M.; Uher, C.; Kanatzidis, M. G. $CsBi_4Te_6$: A High-Performance Thermoelectric Material for Low-Temperature Applications. *Science* **2000**, *287*, 1024−1027.
(8) Island, J. O.; Molina-Mendoza, A. J.; Barawi, M.; Biele, R.; Flores, E.; Clamagirand, J. M.; Ares, J. R.; Sánchez, C.; van der Zant, H. S. J.; D'Agosta, R.; Ferrer, I. J.; Castellanos-Gomez, A. Electronics and Optoelectronics of Quasi-1D Layered Transition Metal Trichalcogenides. *2D Mater.* **2017**, *4*, 22003.
(9) Stolyarov, M. A.; Liu, G.; Bloodgood, M. A.; Aytan, E.; Jiang, C.; Samnakay, R.; Salguero, T. T.; Nika, D. L.; Rumyantsev, S. L.; Shur, M. S.; Bozhilov, K. N.; Balandin, A. A. Breakdown Current Density in H-BN-Capped Quasi-1D TaSe 3 Metallic Nanowires: Prospects of Interconnect Applications. *Nanoscale* **2016**, *8*, 15774−15782.
(10) Liu, G.; Rumyantsev, S.; Bloodgood, M. A.; Salguero, T. T.; Shur, M.; Balandin, A. A. Low-Frequency Electronic Noise in Quasi-1D $TaSe_3$ van Der Waals Nanowires. *Nano Lett.* **2017**, *17*, 377−383.
(11) Balandin, A. A.; Ghosh, S.; Bao, W.; Calizo, I.; Teweldebrhan, D.; Miao, F.; Lau, C. N. Superior Thermal Conductivity of Single-Layer Graphene. *Nano Lett.* **2008**, *8*, 902−907.
(12) Balandin, A. A. Thermal Properties of Graphene and Nanostructured Carbon Materials. *Nat. Mater.* **2011**, *10*, 569−581.
(13) Nika, D. L.; Balandin, A. A. Phonons and Thermal Transport in Graphene and Graphene-Based Materials. *Rep. Prog. Phys.* **2017**, *80*, 36502.
(14) Yue, Y.; Zhang, J.; Xie, Y.; Chen, W.; Wang, X. Energy Coupling across Low-Dimensional Contact Interfaces at the Atomic Scale. *Int. J. Heat Mass Transfer* **2017**, *110*, 827−844.
(15) Ghosh, S.; Bao, W.; Nika, D. L.; Subrina, S.; Pokatilov, E. P.; Lau, C. N.; Balandin, A. A. Dimensional Crossover of Thermal Transport in Few-Layer Graphene. *Nat. Mater.* **2010**, *9*, 555−558.
(16) Wang, Y.; Xu, N.; Li, D.; Zhu, J. Thermal Properties of Two Dimensional Layered Materials. *Adv. Funct. Mater.* **2017**, *27*, 1604134.
(17) Yang, J.; Shen, M.; Yang, Y.; Evans, W. J.; Wei, Z.; Chen, W.; Zinn, A. A.; Chen, Y.; Prasher, R.; Xu, T. T.; Keblinski, P.; Li, D. Phonon Transport through Point Contacts between Graphitic Nanomaterials. *Phys. Rev. Lett.* **2014**, *112*, 205901.
(18) Cai, H.; Chen, B.; Wang, G.; Soignard, E.; Khosravi, A.; Manca, M.; Marie, X.; Chang, S. L. Y.; Urbaszek, B.; Tongay, S. Synthesis of Highly Anisotropic Semiconducting GaTe Nanomaterials and Emerging Properties Enabled by Epitaxy. *Adv. Mater.* **2017**, *29*, 1605551.
(19) Henry, A.; Chen, G. Anomalous Heat Conduction in Polyethylene Chains: Theory and Molecular Dynamics Simulations. *Phys. Rev. B: Condens. Matter Mater. Phys.* **2009**, *79*, 144305.
(20) Liu, J.; Yang, R. Length-Dependent Thermal Conductivity of Single Extended Polymer Chains. *Phys. Rev. B: Condens. Matter Mater. Phys.* **2012**, *86*, 104307.
(21) Liu, J.; Li, T.; Hu, Y.; Zhang, X. Benchmark Study of the Length Dependent Thermal Conductivity of Individual Suspended, Pristine SWCNTs. *Nanoscale* **2017**, *9*, 1496−1501.
(22) Yang, L.; Yang, Y.; Zhang, Q.; Zhang, Y.; Jiang, Y.; Guan, Z.; Gerboth, M.; Yang, J.; Chen, Y.; Greg Walker, D.; Xu, T. T.; Li, D. Thermal Conductivity of Individual Silicon Nanoribbons. *Nanoscale* **2016**, *8*, 17895−17901.
(23) Chen, J.; Zhang, G.; Li, B. A Universal Gauge for Thermal Conductivity of Silicon Nanowires with Different Cross Sectional Geometries. *J. Chem. Phys.* **2011**, *135*, 1−8.
(24) Xiao-Kun, G.; Bing-Yang, C. Thermal Conductivity of Dielectric Nanowires with Different Cross-Section Shapes. *Chin. Phys.* **2007**, *16*, 3777−3782.
(25) Wang, Z.; Mingo, N. Absence of Casimir Regime in Two-Dimensional Nanoribbon Phonon Conduction. *Appl. Phys. Lett.* **2011**, *99*, 101903.
(26) Shi, L.; Li, D.; Yu, C.; Jang, W.; Kim, D.; Yao, Z.; Kim, P.; Majumdar, A. Measuring Thermal and Thermoelectric Properties of One-Dimensional Nanostructures Using a Microfabricated Device. *J. Heat Transfer* **2003**, *125*, 881−888.
(27) Yang, J.; Yang, Y.; Waltermire, S. W.; Gutu, T.; Zinn, A. A.; Xu, T. T.; Chen, Y.; Li, D. Measurement of the Intrinsic Thermal Conductivity of a Multiwalled Carbon Nanotube and Its Contact Thermal Resistance with the Substrate. *Small* **2011**, *7*, 2334−2340.
(28) Prasher, R. Thermal Boundary Resistance and Thermal Conductivity of Multiwalled Carbon Nanotubes. *Phys. Rev. B: Condens. Matter Mater. Phys.* **2008**, *77*, 75424.
(29) Huang, B.-W.; Hsiao, T.-K.; Lin, K.-H.; Chiou, D.-W.; Chang, C.-W. Length-Dependent Thermal Transport and Ballistic Thermal Conduction. *AIP Adv.* **2015**, *5*, 53202.
(30) Hochbaum, A. I.; Chen, R.; Delgado, R. D.; Liang, W.; Garnett, E. C.; Najarian, M.; Majumdar, A.; Yang, P. Enhanced Thermoelectric Performance of Rough Silicon Nanowires. *Nature* **2008**, *451*, 163−167.
(31) Tang, H.; Wang, X.; Xiong, Y.; Zhao, Y.; Zhang, Y. Y.; Zhang, Y. Y.; Yang, J.; Xu, D. Thermoelectric Characterization of Individual Bismuth Selenide Topological Insulator Nanoribbons. *Nanoscale* **2015**, *7*, 6683−6690.
(32) Lindsay, L.; Broido, D. A. Theory of Thermal Transport in Multilayer Hexagonal Boron Nitride and Nanotubes. *Phys. Rev. B: Condens. Matter Mater. Phys.* **2012**, *85*, 35436.
(33) Gu, X.; Li, B.; Yang, R. Layer Thickness-Dependent Phonon Properties and Thermal Conductivity of MoS_2. *J. Appl. Phys.* **2016**, *119*, 85106.
(34) Henry, A.; Chen, G.; Plimpton, S. J.; Thompson, A. 1D-to-3D Transition of Phonon Heat Conduction in Polyethylene Using Molecular Dynamics Simulations. *Phys. Rev. B: Condens. Matter Mater. Phys.* **2010**, *82*, 144308.
(35) Smith, B.; Vermeersch, B.; Carrete, J.; Ou, E.; Kim, J.; Mingo, N.; Akinwande, D.; Shi, L. Temperature and Thickness Dependences of the Anisotropic In-Plane Thermal Conductivity of Black Phosphorus. *Adv. Mater.* **2017**, *29*, 1603756.
(36) Hone, J.; Whitney, M.; Piskoti, C.; Zettl, A. Thermal Conductivity of Single-Walled Carbon Nanotubes. *Phys. Rev. B: Condens. Matter Mater. Phys.* **1999**, *59*, R2514−R2516.
(37) Klemens, P. The Specific Heat and Thermal Conductivity of Graphite. *Aust. J. Phys.* **1953**, *6*, 405.
(38) Pop, E.; Varshney, V.; Roy, A. K. Thermal Properties of Graphene: Fundamentals and Applications. *MRS Bull.* **2012**, *37*, 1273−1281.
(39) Fu, Q.; Yang, J.; Chen, Y.; Li, D.; Xu, D. Experimental Evidence of Very Long Intrinsic Phonon Mean Free Path along the c-Axis of Graphite. *Appl. Phys. Lett.* **2015**, *106*, 31905.
(40) Zhang, H.; Chen, X.; Jho, Y. D.; Minnich, A. J. Temperature-Dependent Mean Free Path Spectra of Thermal Phonons Along the c-Axis of Graphite. *Nano Lett.* **2016**, *16*, 1643−1649.

DOI: 10.1021/acsnano.7b08718
ACS Nano 2018, 12, 2634−2642

(41) Wei, Z.; Yang, J.; Chen, W.; Bi, K.; Li, D.; Chen, Y. Phonon Mean Free Path of Graphite along the c-Axis. *Appl. Phys. Lett.* **2014**, *104*, 81903.
(42) Li, D.; Wu, Y.; Kim, P.; Shi, L.; Yang, P.; Majumdar, A. Thermal Conductivity of Individual Silicon Nanowires. *Appl. Phys. Lett.* **2003**, *83*, 2934−2936.
(43) Hsiao, T.-K.; Chang, H.-K.; Liou, S.-C.; Chu, M.-W.; Lee, S.-C.; Chang, C.-W. Observation of Room-Temperature Ballistic Thermal Conduction Persisting over 8.3-μm in SiGe Nanowires. *Nat. Nanotechnol.* **2013**, *8*, 534−538.
(44) Wei, Z.; Chen, Y.; Dames, C. Negative Correlation between in-Plane Bonding Strength and Cross-Plane Thermal Conductivity in a Model Layered Material. *Appl. Phys. Lett.* **2013**, *102*, 11901.
(45) Hu, Y.; Zeng, L.; Minnich, A. J.; Dresselhaus, M. S.; Chen, G. Spectral Mapping of Thermal Conductivity through Nanoscale Ballistic Transport. *Nat. Nanotechnol.* **2015**, *10*, 701−706.
(46) Lee, J.; Lim, J.; Yang, P. Ballistic Phonon Transport in Holey Silicon. *Nano Lett.* **2015**, *15*, 3273−3279.
(47) Maire, J.; Anufriev, R.; Nomura, M. Ballistic Thermal Transport in Silicon Nanowires. *Sci. Rep.* **2017**, *7*, 41794.
(48) Toberer, E. S.; Zevalkink, A.; Snyder, G. J. Phonon Engineering through Crystal Chemistry. *J. Mater. Chem.* **2011**, *21*, 15843.
(49) Wingert, M. C.; Chen, Z. C. Y.; Kwon, S.; Xiang, J.; Chen, R. Ultra-Sensitive Thermal Conductance Measurement of One-Dimensional Nanostructures Enhanced by Differential Bridge. *Rev. Sci. Instrum.* **2012**, *83*, 24901.
(50) Zhang, Q.; Cui, Z.; Wei, Z.; Chang, S. Y.; Yang, L.; Zhao, Y.; Yang, Y.; Guan, Z.; Jiang, Y.; Fowlkes, J.; Yang, J.; Xu, D.; Chen, Y.; Xu, T. T.; Li, D. Defect Facilitated Phonon Transport through Kinks in Boron Carbide Nanowires. *Nano Lett.* **2017**, *17*, 3550−3555.
(51) Yang, L.; Zhang, Q.; Cui, Z.; Gerboth, M.; Zhao, Y.; Xu, T. T.; Walker, D. G.; Li, D. Ballistic Phonon Penetration Depth in Amorphous Silicon Dioxide. *Nano Lett.* **2017**, *17*, 7218−7225.
(52) Coleman, H. W.; Steele, W. G. *Experimentation, Validation, and Uncertainty Analysis for Engineers*, 3rd ed.; John Wiley & Sons, Inc.: Hoboken, NJ, 2009; pp 29−58.

DOI: 10.1021/acsnano.7b08718
ACS Nano 2018, 12, 2634−2642